Boron induced change of the Eu valence state in $EuPd_3B_x$ ($0 \leq x \leq 0.53$): A theoretical and experimental study

R. Gumeniuk, M. Schmitt, C. Loison, W. Carrillo-Cabrera, U. Burkhardt, G. Auffermann, M. Schmidt, W. Schnelle, C. Geibel, A. Leithe-Jasper, and H. Rosner*

Max Planck Institute for Chemical Physics of Solids, Nöthnitzer Str. 40, 01187 Dresden, Germany

(Received 13 October 2010; published 9 December 2010)

A valence instability of Eu in $EuPd_3B_x$ ($0 \leq x \leq 1$) was discussed controversially in the past. In a joint theoretical and experimental study we investigate a large series of $EuPd_3B_x$ and $GdPd_3B_x$ compounds. Characterization by x-ray diffraction, metallography, energy-, and wavelength-dispersive x-ray spectroscopy as well as chemical analysis determine an existence range of $EuPd_3B_x$ up to $x \leq 0.53$ and $x \leq 0.42$ for the $GdPd_3B_x$ compounds, respectively. Our density-functional-based electronic structure calculation predict a valence change in $EuPd_3B_x$ above $x_c^{DFT} = 0.19 \pm 0.02$ from a nonmagnetic Eu^{3+} state into a magnetic Eu^{2+} state which is reflected in a discontinuity of the lattice parameter. In contrast, the related Gd compounds with a stable Gd^{3+} state exhibit an almost linear behavior of the lattice parameter following Vegard's law. Consistent with the calculations, the x-ray diffraction data show a kink in the lattice parameter for $EuPd_3B_x$ at $x_c^{XRD} = 0.22 \pm 0.02$. X-ray absorption spectroscopy measurements assign this kink to a transition into a heterogeneous mixed valence state for Eu with a critical B content $x_c^{XAS} = 0.22 \pm 0.03$. The observed change in the mean Eu valence from Eu^{3+} ($x \leq 0.2$) toward $Eu^{2.5+}$ ($x = 0.5$) is supported by magnetic susceptibility and specific-heat data.

DOI: 10.1103/PhysRevB.82.235113 PACS number(s): 71.20.Eh, 71.15.Mb, 75.20.Hr

I. INTRODUCTION

Valence instabilities observed in rare-earth (*RE*) $4f$ electron systems have been of considerable interest and topic of numerous concerted experimental and theoretical investigations. In solids the *RE* metals are mostly trivalent in the standard state. Exceptions to the rule are Ce which has also been found in a tetravalent state and Sm, Eu, Tm, or Yb with divalent states, respectively, moreover also in mixed or intermediate valences. The divalent and tetravalent states are often energetically stabilized by the formation of a full, half-full, or empty $4f$ shell. In fact, of the aforementioned metals europium and ytterbium are the only lanthanide metals which are divalent ($4f^7$;$4f^{14}$) in their elemental metallic standard state,[1] as well as in some alloys and intermetallic compounds. In that case their crystal chemistry strongly resembles that of the alkaline-earths metals, typically influenced by the large radii of the ions. Nevertheless, in many systems Eu and Yb are found to be in a trivalent ($4f^6$;$4f^{13}$) state similar to the rest of the rare-earth metals.[2] The physical properties of Yb and Eu are significantly different in the two states, namely, Eu^{2+} ($S=7/2$, $L=0$) and Yb^{3+} ($S=1/2$, $L=3$) carrying a high magnetic moment ($J=7/2$) compared to Eu^{3+} with nonmagnetic ground state ($S=3$, $L=3$, $J=L-S=0$) and Yb^{2+} ($S=L=J=0$). Thus, not only the crystal chemistry depends crucially on the $4f$ valence but also the related electronic and magnetic properties.

In many cases, a deviation from the typical trivalent state of the *RE* component can already be suspected from a deviation of the unit-cell volume of a specific compound from the expected volume decrease within the *RE* compound series according to the lanthanide contraction rule. The valency of several *RE* species in a compound is determined by many factors like the local environment (determining the crystal-field splitting), the electronegativity and the concentration of the alloying partners[3–5] in the compound as well as external parameters such as temperature, pressure, and magnetic field.[6] Therefore, a typical approach to study *RE* valence changes is the successive variation in these relevant factors in a systematic way.

This has been done in the $REPd_3$ systems (cubic, Cu_3Au type of structure) with $CePd_3$ being an archetype of an intermetallic compound exhibiting an intermediate valence of Ce.[7,8] Despite the rather simple cubic crystal structure, members of this family of compounds exhibit exiting physical properties which have been studied for several decades and still fuel many scientific activities.[9–15] The fact that Eu in phases with the Cu_3Au crystal structure is prone to valence transitions and still merits detailed studies has been recently demonstrated by Pandey *et al.*[16] for $Eu_{0.4}La_{0.6}Pd_3$ and $Ce_{0.5}Eu_{0.5}Pd_3$.[17] For these compounds valence instabilities of Eu are discussed as being correlated with "negative pressure" induced by substitution of Eu by La. In case of a substitution of Eu by Ce no lattice expansion has been observed.

The insertion of boron in $REPd_3$ compounds had been studied by Dhar *et al.* systematically using x-ray diffraction (XRD) and magnetic-susceptibility measurements.[18–20] An increase in the lattice parameter under B insertion was observed for the *RE* series $REPd_3B_x$ as reported in Ref. 18. Above a certain concentration x, depending on the *RE* metal, a further increase in the B content leaves the lattice parameter unaffected. In addition, for *RE*=Eu and Yb a pronounced anomaly in the lattice parameter compared to the other *RE* compounds was found. This peculiarity lead to further studies on the Eu compound based on Mössbauer and x-ray absorption near-edge-structure spectroscopy (XANES),[21–23] reporting a decrease in the mean Eu valence ν for $x > 0.25$ connected with the formation of a heterogeneous mixed valence state. Furthermore, for $LaPd_3$ no variation in the lattice parameter was observed at all,[18] up to the fully stoichiometric $LaPd_3B$.

Stimulated by the difficulties to interpret these effects based on the reported data, (as, e.g., the critical B concentration for the transition is inconsistent) we have recently studied the electronic structures of intermetallic borides $RE\mathrm{Pd}_3\mathrm{B}_x$ within the density functional theory using the local spin-density approximation with correlations (LSDA+U) and coherent-potential approximation (CPA) for the whole series from RE=La to Lu as a function of the boron content.[24] In contrast to the earlier studies, a regular increase in the lattice parameters has been observed in the calculations for the whole range of $0 \leq x \leq 1$. Moreover, the calculated lattice parameters obtained for all $RE\mathrm{Pd}_3\mathrm{B}$ compounds are significantly higher than the experimental lattice parameters,[18] questioning the reported synthesis of stoichiometric compounds $RE\mathrm{Pd}_3\mathrm{B}$. In this context, we could unambiguously show by detailed experimental studies based on powder XRD, metallography, and electron microprobe analysis that boron cannot be inserted into LaPd_3 under equilibrium conditions. Instead, in a sample with nominal $\mathrm{LaPd}_3\mathrm{B}$ stoichiometry, the precipitation of LaB_6 crystals in a LaPd_3 matrix was observed.

The impossibility to insert B in the LaPd_3 compound enforces the question, whether similar effects also appear in the other compounds of the series resulting in a partial insertion of B only. Thus, the inconsistent reports about valence changes could have their origin in different sample compositions.

Since we conclude from our electronic-structure calculations a trivalent state for Eu in EuPd_3 and a divalent state in $\mathrm{EuPd}_3\mathrm{B}$, a detailed theoretical study of $\mathrm{EuPd}_3\mathrm{B}_x$ was started together with careful sample preparation and characterization to reinvestigate a possible valence instability in $\mathrm{EuPd}_3\mathrm{B}_x$.

II. METHODS

A. Calculational

For the electronic structure calculations the full-potential nonorthogonal local-orbital minimum basis scheme FPLO (version: FPLO5.00-19) within the LSDA was used.[25] In the scalar relativistic calculations the exchange and correlation potential of Perdew and Wang was chosen.[26] As basis set the following semicore/valence and polarization states were taken into account: Eu(Gd)($4d4f5s5p$)/($6s6p5d$), Pd($4s4p$)/($5s5p4d$) and B($2s2p3d$). All lower-lying states were treated as core states in a fully relativistic way.

To take into account the strong correlation in the Eu $4f$ shell in a mean-field like approximation we performed LSDA+U calculations[27] with the on-site Coulomb repulsion U=8 eV (in the atomic limit for the double-counting scheme) and the on-site exchange J=1 eV. This corresponds to the Slater parameters F_0=8 eV, F_2=11.91 eV, F_4=7.96 eV, and F_6=5.89 eV typical for $4f$ elements.[28] The variation in U between 6 and 8 eV and J between 0 and 1 eV does not change the results qualitatively.

To model the gradual, disordered insertion of B from EuPd_3 to $\mathrm{EuPd}_3\mathrm{B}$, the CPA (Ref. 29) was used. For the ordered cases (x=0, a supercell with x=0.5 and x=1) the CPA calculations were compared to usual ordered structure calculations using the Blackman-Esterling-Berk (BEB) (Ref. 30) approach to check the accuracy.

B. Experimental

Samples were synthesized from Eu (ChemPur, 99.9 wt %, distilled in vacuum prior to use), Gd (Ames, 99.9 wt %), Pd (foil, ChemPur, 99.9 wt %) and crystalline B powder (powder $<$100 μm, Alfa Aesar, 99.995 wt %). Samples of about 0.75 g each were prepared by arc-melting (Eu/Gd)Pd_x master alloys with PdB_y alloys. They were remelted several times (weight losses $<$1%). All these manipulations were performed inside an argon filled glove box system (O_2 and H_2O partial pressures $<$1 ppm).

For homogeneity annealing, each sample was welded inside a Ta ampoule which was then sealed in quartz ampoules and kept at 950 °C for 10 days. Samples with Boron content $x>0.6$ were additionally annealed at 1000 °C for 4 days. Finally the ampoules were quenched in cold water. Because of the ductility of the samples stress annealing of powders of all samples was performed at 950 °C for 3 h to obtain powder patterns with better quality (sharper diffraction peaks).

Phase identification was performed on the basis of powder patterns obtained with a HUBER G670 imaging plate Guinier-camera equipped with a Ge monochromator and operated with Cu $K\alpha_1$ radiation (λ=1.54056 Å). For powder XRD, the samples were crushed and powdered under argon gas. The samples were then loaded between two polyimide foils in an aluminum holder with a rubber sealing to exclude air and moisture, and subjected to XRD analysis immediately afterward. Phase analysis was performed using the WINXPOW (STOE) program package.[31] The lattice parameters were refined by least-squares fitting of powder data with Ge as internal standard (a=5.6569 Å) using the WINCSD software.[32]

For metallographic examinations, pieces of about 3 mm were cut from the annealed samples. They were mounted in conductive resin. Grinding was performed on abrasive papers (500 and 1000 grit silicon carbide) and a water-free lubricant. Polishing was done using slurries of 9 and 3 μm diamond powder in water-free lubricants. All experimental steps were performed in an argon-filled glove box. The homogeneity of the microstructures was examined optically (Zeiss Axioplan 2). The compositions of the observed phases were analyzed by wavelength-dispersive x-ray spectroscopy (WDXS) (Cameca SX 100) on an electron-probe microanalyzer and by energy-dispersive x-ray spectroscopy (EDXS) methods [EDAX Phoenix system with Si(Li) detector on a scanning electron microscopy].

The WDXS measurements on selected $\mathrm{GdPd}_3\mathrm{B}_x$ and $\mathrm{EuPd}_3\mathrm{B}_x$ compounds were performed up to the maximal boron solubility (see Fig. 3). This corresponds to a maximal content of approximately only 1 wt % boron. For both systems the $RE\mathrm{Pd}_3$ phase was used as standard material for the rare-earth element and Pd. The intensities of the RE L_α line (Eu L_α: 5846 eV; Gd L_α: 6057 eV) and the Pd L_α line (2839 eV) were measured. The monochromator crystals LPC3 (Mo/B_4C multilayer; $2d$=20 nm), LPET [pentaerythritol, $2d$=0.87 nm] and LiF ($2d$=0.4 nm) were used for the B, Pd, and RE lines. $\mathrm{Pd}_3\mathrm{B}$ was used as standard for the B K_α

line (183 eV). The matrix correction model according to Pouchou and Pichoir[33] was applied to calculate the chemical composition. Different conditions have been applied for the measurement of the x-ray line of the heavy elements and boron. An acceleration voltage of 25 kV and a current of 20 nA results in count rates of ~10 000 cps and 5000 cps for the Pd and the *RE* line, respectively. The boron line was measured by the area intensity method. Here, we applied 7 kV, 100 nA and a very long dwell time of 30 s to handle the small intensities. Additionally, the $RE\mathrm{Pd}_3$ standards gave the possibility to determine the background intensity at the energy of the B K_α line. Compositions of some samples as well as all standards were established by chemical analyses using inductively coupled plasma optical emission spectrometry (VISTA RL, Varian).

Samples for electron diffraction (ED) were prepared by crushing the sample in a mortar. Sample particles were deposited on a carbon film sustained by a copper net. The selected area electron diffraction patterns were obtained using an electron microscope Tecnai 10 equipped with a charge coupled device camera (TemCam-F224HD, MTVIS).

The Eu L_{III} x-ray absorption spectra (XAS) were recorded in transmission arrangement at the EXAFS beamlines A1 and E4 of HASYLAB at DESY, Hamburg Germany. The wavelength selection was realized by means of a Si (111) double crystal monochromator, which yielded an experimental resolution of ≈2 eV (full width at half maximum) at the Eu L_{III} threshold of 6977 eV. Experimental data were measured using EuF_3 as an external reference compound. The obtained x-ray absorption spectra were analyzed by a least-squares fitting procedure to obtain the Eu valence ν according to $\nu=2+I(\mathrm{Eu}^{3+})/[I(\mathrm{Eu}^{2+})+I(\mathrm{Eu}^{3+})]$, where $I(\mathrm{Eu}^{2+})$ and $I(\mathrm{Eu}^{3+})$ are the intensities of the Eu^{2+} and the Eu^{3+} peak, respectively.[34–36]

III. RESULTS AND DISCUSSION

A. Calculations

To investigate a possible valence instability in the $\mathrm{EuPd_3B}_x$ compounds depending on the B content x, LSDA $+U$ calculations for the two ordered extreme cases $x=0$ and $x=1$ were carried out. However, $\mathrm{EuPd_3B}$ represents a fictitious compound since no complete occupation of the B position can be experimentally achieved (see below). A discussion of the underlying crystal structure as well as preferential site occupation by the B atoms has been given in a previous publication.[24] The resulting densities of states (DOS) are depicted in Fig. 1. In both compounds the valence band is mainly formed from (nonpolarized) Pd 4*d* states. The contributions from Pd 5*p* and 5*s* as well as Eu 5*d* and 6*s* states are very small and can be neglected. The B states in $\mathrm{EuPd_3B}$ appear below −5 eV. Thus, the main differences between both compounds are due to the Eu 4*f* states and the position of the Fermi energy. The strongly localized 4*f* states yield sharp peaks in the density of states. For $\mathrm{EuPd_3}$ we find these peaks in the majority channel at the lower end of the valence band and an unoccupied 4*f* state at about 1 eV above the Fermi energy. In the minority-spin channel all 4*f* states are unoccupied as expected. Evaluating the occupation of the 4*f* orbital, $\mathrm{EuPd_3}$ is in a $4f^6$ state. Since the valence band is unpolarized, a nonmagnetic ground state can be expected due to the Hund's rules ($J=L-S=0$).

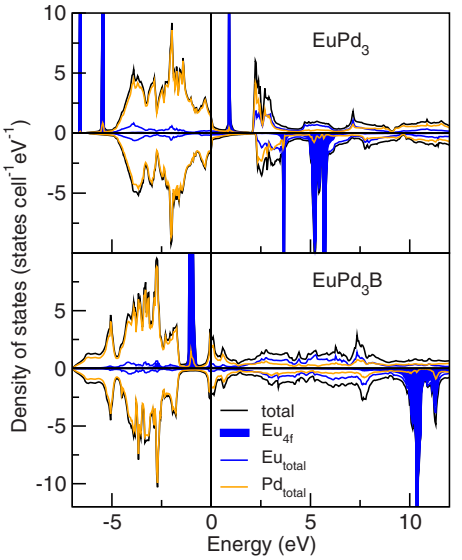

FIG. 1. (Color online) Calculated density of states for $\mathrm{EuPd_3}$ (top) and $\mathrm{EuPd_3B}$ (bottom). Beside the Eu 4*f* states, $\mathrm{EuPd_3}$ shows a symmetric density of states for the two spin channels. In $\mathrm{EuPd_3B}$ the majority-spin channel shows fully occupied 4*f* states.

In $\mathrm{EuPd_3B}$, connected with the insertion of B, the 4*f* states of the majority spin channel become fully occupied. These strongly localized states are placed at about −1 eV. The 4*f* states of the minority-spin channel remain unoccupied and are shifted upwards to 10.5 eV, according the energy difference $\Delta E\sim U+I$ from the on-site repulsion U and the exchange split I (compare energy difference of the unoccupied majority and minority 4*f* states in $\mathrm{EuPd_3}$ and $\mathrm{EuPd_3B}$, see Fig. 1). This results in a magnetic Eu $4f^7$ state.

Following the question, how the 4*f* occupation develops with x in more detail, we model a successive insertion of B from $\mathrm{EuPd_3}$ to $\mathrm{EuPd_3B}$ using CPA calculations. While the disorder of the insertion is covered by the CPA, a possible dynamic mixed valence scenario for Eu cannot be simulated, since a fractional occupancy of orbitals is suppressed by the LSDA$+U$ approach, which favors full polarization. Furthermore the combination of the LSDA$+U$ and CPA method results in a complex potential surface with several local minima, causing difficulties to find the correct global minimum. Considering the difficulty of multiple solutions (depending on numerical parameters in the CPA approach), we compared LSDA$+U$ results for the ordered structures ($x=0$, $x=0.5$ and $x=1$) with the corresponding BEB results and with CPA calculations for similar concentration ($x=0.01$, $x=0.5$ and $x=0.99$). The obtained DOS show only minor differences at the lower end of the valence band and in the unoccupied states. Comparing optimized lattice parameters using the different approaches leads essentially to the same results. Thus, the CPA approach is well controlled and yields justified results.

We optimized the crystal structure (with the lattice parameter as the only free parameter) for several different B concentrations and evaluated the electron population of the Eu

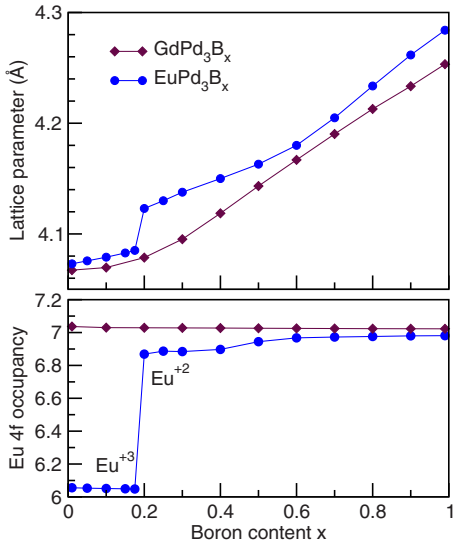

FIG. 2. (Color online) Optimized theoretical lattice parameter and $4f$ occupation for different B concentrations in $EuPd_3B_x$ and $GdPd_3B_x$. In $EuPd_3B_x$ the lattice parameters show a jump at $x \approx 0.2$. For the same B concentration a change from a trivalent to a divalent Eu state is observed.

states. The dependence of the lattice parameters a on the B content x (see Fig. 2) shows a sudden increase at $x_c^{\mathrm{DFT}} = 0.19 \pm 0.02$. This anomaly of the lattice parameter corresponds to a volume change of about 2.6% and is accompanied by a drastic change in the Eu $4f$ occupation from the trivalent to the divalent state. In contrast, the reference system $GdPd_3B_x$ with a half filled $4f$ shell, shows a stable $4f^7$ state under B insertion and a smoothly increasing lattice parameter as one might expect from Vegard's law.

B. Homogeneity ranges of $GdPd_3B_x$ and $EuPd_3B_x$

To establish the extensions of the homogeneity ranges of $GdPd_3B_x$ and $EuPd_3B_x$ several samples have been synthesized. Phase analysis based on powder XRD as well as EDXS show the samples $GdPd_3B_x$ ($x \leq 0.4$) and $EuPd_3B_x$ ($x \leq 0.53$) to be single phase overall. Compositions of selected samples obtained from chemical analysis are in good agreement with nominal ones in the whole range of x (see Ref. 37). In Fig. 3 the dependence of the lattice parameters of $EuPd_3B_x$ and $GdPd_3B_x$ as a function of the B content x is depicted. No increase in the lattice spacing is observed for $x \geq 0.42$ in the case of $GdPd_3B_x$ and for $x \geq 0.53$ for $EuPd_3B_x$, thus indicating the solubility limit of boron in the compounds.

Accordingly, in the metallographic and powder XRD analysis of the samples with nominally higher boron content, formation of GdB_6 and EuB_6 as additional phases is observed. Thus, at the experimental conditions employed in this study, the formation of fully stoichiometric $REPd_3B$ (RE =Eu,Gd) compounds can be ruled out. Alloying boron to $GdPd_3$ results in a linear expansion of the lattice up to the solubility limit (see Fig. 3). For the $EuPd_3B$ system a change in slope of the otherwise linear lattice expansion can be easily seen at a threshold composition of about $EuPd_3B_{0.22(2)}$.

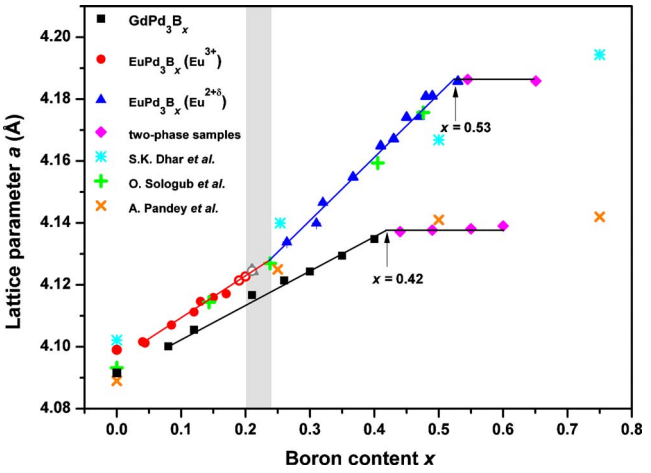

FIG. 3. (Color online) Experimentally observed variation in the primitive unit cell parameter a in $REPd_3B_x$ (RE=Eu,Gd) versus boron concentration x. For comparison the experimental results from Refs. 19, 39, and 40 are included. Samples with $x=1$ reported by Dhar *et al.* and Pandey *et al.* are not shown since their lattice parameter do not increase further compared to $x=0.75$.

There, a deviation from the volume increase merely induced by the introduction of boron becomes clearly visible if compared to $GdPd_3B_x$ where no anomalies are discernible. This behavior can be attributed to a change in the valence of Eu which is accompanied by a drastic increase in the ionic radius (see above and discussion) and therefore results in a more progressive lattice expansion.

It is interesting to compare these findings with the results of Dhar *et al.*[18,19,38] Judging from a figure in their publication, where they show the lattice parameter of as-cast samples as a function of the B content, the authors observed an expansion of the lattice in the $EuPd_3B_x$ system up to a nominal composition with $x=0.75$. Exceeding this filling fraction no more expansion is observed until stoichiometric $EuPd_3B$ with $a=4.196$ Å is reached. In case of the $GdPd_3B_x$ system, despite the same characteristics, the expansion stops at a much lower nominal value $x \approx 0.35$ and the lattice parameter stays constant up to nominal $GdPd_3B$ with a =4.146 Å [Ref. 18; compare with $a=4.1372(2)$ Å of $GdPd_3B_{0.44}$ in our study].

Different to their results we do not observe an expansion of the lattice beyond $x=0.75$ for the Eu compounds (see above). Our findings are also substantiated by a recent study of phase equilibria in the Eu-Pd-B ternary system and of $GdPd_3B_x$ solid solution.[39,40] Relevant lattice parameters as a function of boron content are included in Fig. 3. A comparison of lattice parameters suggests that Dhar *et al.*, because they took the nominal B concentration, overestimated the real B content of the $REPd_3B_x$ phase in their samples. At higher B contents we find a phase separation into $EuPd_3B_{0.53}$ and EuB_6 instead of the stoichiometric compound $EuPd_3B$ with full occupancy of the $1b$ site as suggested by Dhar *et al.*

Moreover, in the present study we can clearly distinguish (already from inspection of the trend of the lattice spacing) between effects due to boron induced expansion and the change in europium valence. This is manifested in the distinct change in slope (see above) of the expansion. As de-

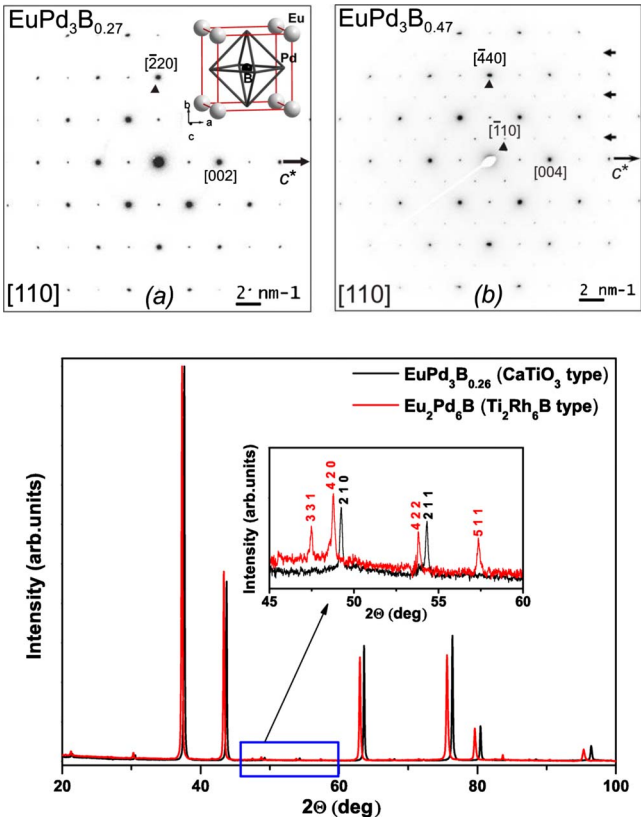

FIG. 4. (Color online) Upper panel: ED pattern for $EuPd_3B_x$ with $x=0.27$ (a) and $x=0.47$ (b). Arrows point to reflections indicating lattice parameter doubling. Lower panel: XRD pattern for two different samples showing $CaTiO_3$ and Ti_2Rh_6B type of structure. The superstructure reflections are magnified in the inset.

picted in Fig. 3 and listed in the supplementary material (see Ref. 37), in our study $EuPd_3B_{0.53}$ represents the compound with the largest lattice parameter of $a_P=a'/2=4.1857(8)$ Å and the highest boron content.

Interestingly, a close inspection of the powder XRD and ED pattern of samples with B content $x>0.35$ revealed beside the fundamental reflections of antiperovskite $EuPd_3B_x$ the occurrence of weak additional reflections (see Fig. 4 top). Since metallographic analysis revealed the samples to be single phase, these reflections have to be attributed to subtle changes in the crystal structure of $EuPd_3B_x$. The powder XRD pattern could be satisfactorily indexed and refined based on a cubic face-centered lattice with lattice parameter $a'=2a_P=8.3509(3)$ Å which corresponds to a doubling of the original lattice parameter a_P. This resembles the crystal chemical behavior often observed in the archetypal field of oxygen-based perovskites AMO_3, when the arrangement of chemically different M cations gives rise to the formation of so-called double perovskites with a formula of $A_2MM''O_6$. There, the arrangements of the M, M'' cations enable different types of sublattices, thus strongly influencing the crystallographic and physical properties. Several cation ordering schemes, their symmetry relations and important implications for material science have been exhaustively studied in literature.[41–43] With respect to the crystallographic observations on intermetallic $EuPd_3B_x$, the rock-salt-type sublattice is of importance (again we have to think of an antiperovskite-type arrangement, where formally Pd atoms occupy the O site, boron represents the M cation, and Eu the large electropositive element A). Indeed, passing the threshold boron concentration of $x>0.35$, a crystal structure evolves with an fcc ordering of empty $[Pd_6]$ and filled $[Pd_6B]$ octahedra reflected in the doubling of the lattice parameter and adopting of the space group $Fm\bar{3}m$ (see Fig. 4 and Table I). Similar structural motives, though without long or short-range order are observed in the solid solution of B in fcc Pd metal.[44] To be analogous to the double perovskite picture this means that the M'' position remains empty (i.e., Eu_2Pd_6B which corresponds to $EuPd_3B_{0.5}$). A similar complication of the antiperovskite crystal structure (as a function of boron concentration) has been recently discovered for Ti_2Rh_6B and $ScIr_3B_x$.[45] No such superstructure formation is observed in the $GdPd_3B_x$ series.

The DOS for the superstructure of $EuPd_3B_{0.5}$, depicted in Fig. 5, is similar to that of the fictitious $EuPd_3B$ (compare Fig. 1). The valence band is dominated by Pd states between −5 eV and the Fermi energy. Below −5 eV a small separated, narrow band of Pd and B hybrid states is formed, typical for the family of $REPd_3B$ compounds and also present for $EuPd_3B$ centered at an energy of −9 eV (not shown).[46] The occupation of Eu $4f$ states in the compound is similar to the scenario in $EuPd_3B$ with a fully occupied majority-spin channel and an unoccupied minority spin channel. The observation of small volume differences between boron filled and unfilled Pd_6 octahedra in the superstructure of $EuPd_3B_{0.5}$ is in accord with a 136 meV lower total energy for the superstructure with slightly different filled and unfilled octahedra volume and a structure with uniform octahedra. The volume alteration causes no significant differences in the density of states down to −5 eV.

In contrast to the B-ordered LSDA+U calculations of the superstructure, the B disorder taken into account in the CPA approach influences mainly the Pd-B hybrid states at the lower end of the valence band. As a result, these states are

TABLE I. $EuPd_3B_{0.47}$ crystallizes in the space group $Fm\bar{3}m$ with a lattice parameter $a=8.3510(2)$ Å. (The powder sample was measured using Cu K_{α_1} radiation with a wavelength of $\lambda=1.54056$ Å and refined up to an R-factor of 0.042 fitting the full profile.) * Full occupation for Eu and Pd; B occupation 0.96(5).

Atom	Site	x/a	y/a	z/a	B_{iso}
Eu	8c	1/4	1/4	1/4	0.61(1)
Pd	24e	0.2556(6)	0	0	1.11(2)
B*	4b	0	0	0	2.6(8)

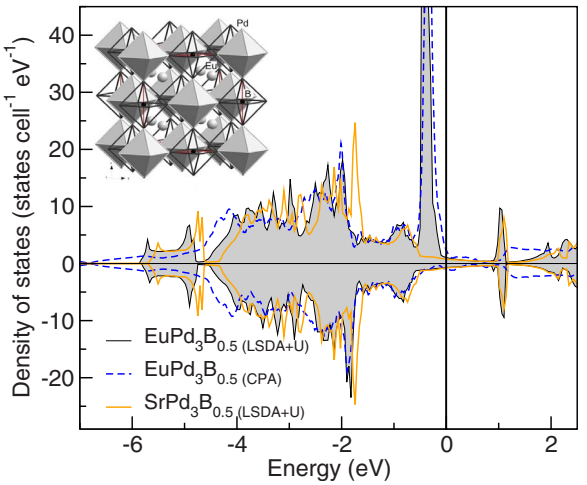

FIG. 5. (Color online) Comparison of the density of states for the B ordered superstructure $EuPd_3B_{0.5}$ (LSDA+U), the B disordered $EuPd_3B_{0.5}$ (CPA) and the related ordered superstructure of $SrPd_3B_{0.5}$. Inset: crystal structure of the ordered superstructure.

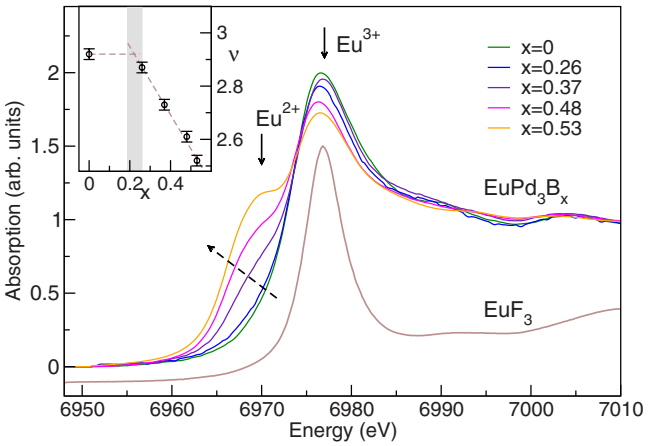

FIG. 6. (Color online) Measured Eu L_{III} XAS spectra of $EuPd_3B_x$ for different B contents in comparison to the reference compound EuF_3. The relation between contributions originating from Eu^{2+} and Eu^{3+} changes with increasing B content. The broken arrow points in direction of decreasing Eu valence (increasing B content x). Inset: Development of the mean Eu valence ν as a function of the B content x.

broadened closing the gap to the rest of the valence band.

Comparing the results of the electronic-structure calculations for $EuPd_3B_{0.5}$ to the related compound $SrPd_3B_{0.5}$,[46] we find a very similar band shape. For $SrPd_3B_{0.5}$, beside a scaling of the bandwidth due to the different lattice parameter, just the sharp peaks of the localized $4f$ states are missing, implying a negligible influence of the Eu $4f$ states on the Pd and B states.

C. Eu L_{III} XAS

The x-ray absorption spectra of selected $EuPd_3B_x$ samples near the Eu L_{III} edge are presented in Fig. 6. The spectrum of $EuPd_3$ is dominated by the contribution of the $4f^6$ state (Eu^{3+}) which is shown by the comparison with the spectrum of the reference compound EuF_3.

The increase in the B content x leads to an increase in the spectral weight of the structure at about 6969 eV below the Eu^{3+} peak at about 6977 eV, indicating increasing contributions of the $4f^7$ state. The spectra of $EuPd_3B_x$ for $x \geq 0.2$ could be successfully deconvoluted, resulting in a mean Eu valence ν up to +2.52 for $x=0.53$. Samples with nominally higher boron contents were not measured due to formation of the EuB_6 impurity phase which contains europium in its divalent state.

The mean Eu valence ν deduced from these measurements is given in Table II and plotted as a function of the boron concentration in the inset of Fig. 6. From a linear extrapolation of $\nu(x)$ we determine a critical B content $x_c^{XAS}=0.22\pm0.03$ for the onset of the Eu mixed valence behavior. This result is well in line with the x-ray diffraction analysis (see previous section) that yielded a kink of the lattice parameter as a function of x at $x_c^{XRD}=0.22\pm0.02$.

Eu systems with nonintegral valence can usually be classified in two different categories: valence fluctuating systems or heterogeneous mixed valence systems. In the former ones all Eu atoms present the same, noninteger valence, which is strongly increasing with decreasing temperature. Typical examples are $EuCu_2Si_2$ (Ref. 47) and $EuPd_2Si_2$.[48] In contrast, the heterogeneous mixed valence systems present an ordered or disordered static distribution of two or more different Eu-valence states, where the mean Eu valence is usually not very dependent on temperature. We therefore investigated the T dependence of ν (see Fig. 7) and found the mean Eu valence to be almost T independent, clearly indicating a heterogeneous mixed valence state in this $EuPd_3B_x$ series, in accordance with the observation of two Mössbauer lines by Dhar *et al.*[21]

D. Magnetic susceptibility

The temperature dependence of the inverse magnetic susceptibilities in high magnetic fields ($\mu_0 H=3.5$ T) of four $EuPd_3B_x$ samples is depicted in Fig. 8. The overall behavior is similar to that reported by Malik *et al.*[23] In accordance with literature data[49,50] $EuPd_3$ shows a Van-Vleck paramagnetic behavior with a temperature independent susceptibility at low temperatures due to the singlet $^7F_0$ ($4f^6$) state of Eu^{3+}. Another sample from the homogeneity region with slightly higher Pd-content $Eu_{0.96}Pd_{3.04}$ shows almost identical magnetic behavior (not depicted in Fig. 8).

TABLE II. Mean Eu valence ν obtained from a deconvolution of the measured XAS spectra. The numerical errors from the fitting procedure can be estimated to be around ±0.02.

Boron content, x	0	0.26	0.37	0.48	0.53
Eu valence, ν	2.92	2.87	2.73	2.61	2.52

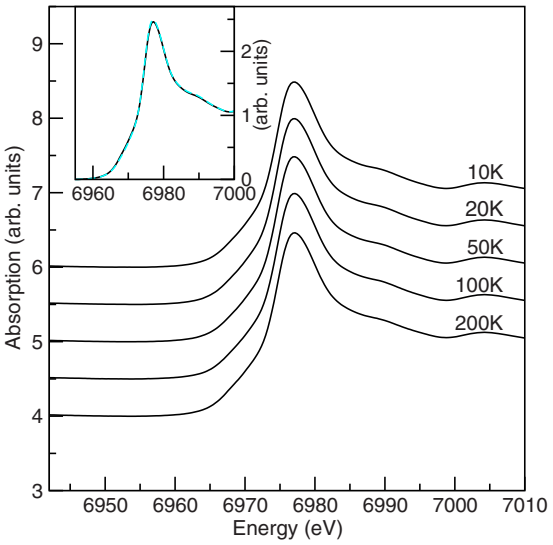

FIG. 7. (Color online) Temperature dependence of the measured Eu L_{III} XAS spectra for $EuPd_3B_{0.32}$ and direct comparison (inset) of the XAS spectra for the maximal measured temperature difference.

In good accordance with the Eu L_{III} XANES measurements the sample $EuPd_3B_{0.26}$ already shows an additional "Curie tail" at low temperatures which can be attributed to the presence of a small amount ($\approx 5\%$) of Eu^{2+} ions.

For further increasing B concentration also the susceptibility at high temperatures is strongly increased, which is obviously connected with the Curie-Weiss-type contribution of the Eu^{2+} $4f^7$ state becoming dominant up to the highest investigated temperatures. For $x \geq 0.37$ the $1/\chi(T)$ versus T plot shows a Curie-Weiss-type behavior with a change in the slope around 100 K. Above 100 K both the Eu^{2+} and the Eu^{3+} contribute to this slope while below 100 K only the Eu^{2+} contributes to the slope since there the Van-Vleck contribution of Eu^{3+} is T independent. For the $EuPd_3B_{0.48}$ sample the slope below 100 K results in an effective moment $\mu_{\mathrm{eff}}=5.0\ \mu_B$/f.u., which corresponds to a Eu^{2+} fraction of $\approx 40\%$, in nice agreement with the results from the XAS L_{III} measurements. Thus, for $x \geq 0.26$ the susceptibility of

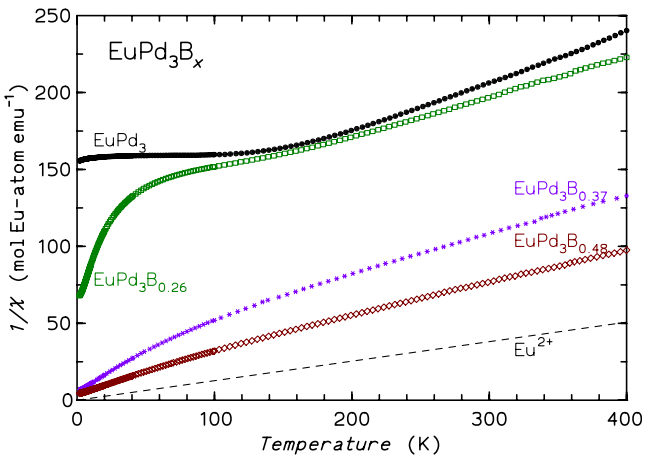

FIG. 8. (Color online) Inverse magnetic susceptibility of different $EuPd_3B_x$ compounds.

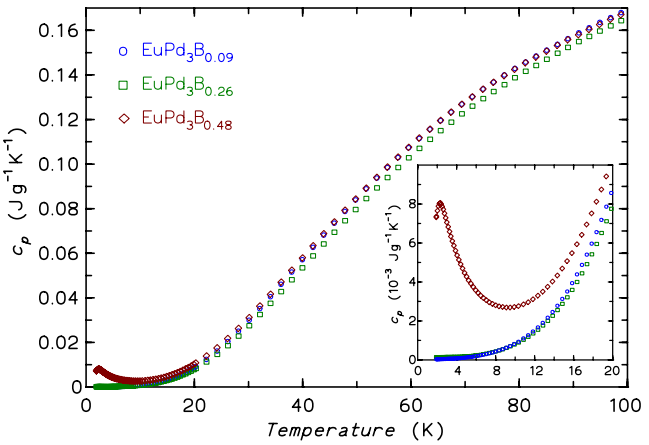

FIG. 9. (Color online) Specific heat for compounds with different B content. The inset shows a magnification of data at the lowest temperatures.

$EuPd_3B_x$ is seemingly just the sum of an Eu^{2+} and an Eu^{3+} contribution with T independent weights, giving a further support for the presence of a heterogeneous mixed valent Eu state. In contrast a valence fluctuating state is characterized by a maximum in $\chi(T)$ at a temperature corresponding to the $Eu^{3+}-Eu^{2+}$ excitation energy.

E. Specific heat

In Fig. 9 the specific-heat capacity of three selected samples is depicted. The compounds $EuPd_3B_{0.04}$ and $EuPd_3B_{0.26}$ show no magnetic contributions. However, in $EuPd_3B_{0.26}$ traces of a Schottky anomaly can be discerned. With increasing external magnetic field its magnetic entropy is shifted to higher temperatures due to the further splitting of the level system. However, the entropy is less than 1% of the one expected for a pure Eu^{2+} state (R ln 8). This anomaly is much more pronounced in $EuPd_3B_{0.48}$ where its maximum is located at 2.3 K close to an anomaly resembling an antiferromagnetic ordering at 1.7 K reported by Dhar *et al.* for $x=0.5$. The maximum moves to only slightly higher temperatures with increasing external field, supporting the presence of short range order. Subtracting now the c_p of the $EuPd_3B_{0.04}$ from the $EuPd_3B_{0.48}$ we find an integrated entropy of 0.8 R, which represents only 38% of the magnetic entropy expected for a Eu^{2+} multiplet, in favorable agreement with 40% Eu^{2+} fraction deduced from the XAS measurements. The fact that the entropy for this Eu^{2+} fraction is already recovered at low temperatures indicates that these Eu^{2+} ions are in a stable, nonfluctuating valence state.

IV. SUMMARY

Stimulated by the controversial debate about the structural, electronic, and magnetic properties of $REPd_3B_x$ compounds,[18,19,21–23] we reinvestigated a large series of $EuPd_3B_x$ and $GdPd_3B_x$ compounds in a joint theoretical and experimental study.

Starting with density-functional-based electronic-structure calculations, they predict a lattice anomaly in $EuPd_3B_x$ for

$x_c^{DFT}=0.19\pm0.02$ which is caused by a change in the Eu $4f$ occupation. This change drives the system from a nonmagnetic Eu^{3+} to a magnetic Eu^{2+} state. In contrast, the calculations for the related $GdPd_3B_x$ reference compounds yield a stable Gd^{3+} valence state and thus a continuous, almost linear behavior of the lattice parameters in line with Vegard's law. It is generally known that present-day DFT calculations have difficulties with respect to the precise description of strongly correlated, in particular, with intermediate or mixed valent $4f$ systems. This general problem inspired us to challenge our theoretical results by an extended experimental study.

Altogether, our experimental investigations confirm a valence transition of Eu upon B insertion in $EuPd_3B_x$. However, instead of a transition from a trivalent to a purely divalent Eu state we observe a transition to a heterogeneous mixed valent state as reported earlier by Dhar *et al.*[21] In our extensive study of more then 20 (10) Eu (Gd) compounds with different B content we could widely profit from the major improvements in synthesis and characterization techniques in the past years. The careful characterization by a combination of x-ray diffraction, metallography, energy-, and wavelength-dispersive x-ray spectroscopy and chemical analysis allowed us to determine precisely (i) the existence range of $EuPd_3B_x$ up to $x\leq0.53$ and $x\leq0.42$ for the $GdPd_3B_x$ compounds, respectively; and (ii) the critical B concentration $x_c^{XRD}=0.22\pm0.02$ for the onset of the valence transition in $EuPd_3B_x$. For higher B concentration than $x=0.53$ ($x=0.42$) the lattice parameter stays constant and additional phases precipitate, which is mainly $Eu(Gd)B_6$, similar to the formation of LaB_6 in $LaPd_3B_x$.

Consistent with the calculated $x_c^{DFT}=0.19\pm0.02$, the x-ray diffraction data show an anomaly of the lattice parameter for $EuPd_3B_x$ at $x_c^{XRD}=0.22\pm0.02$ while continuously increasing lattice parameters for $GdPd_3B_x$ are found up to the solubility limit of B in the compounds. However, in contrast to the calculationally predicted jump in the lattice parameters of $EuPd_3B_x$ we observe a less pronounced anomaly, namely a kink between two regions of linear behavior.

To unravel the origin of this anomaly, we performed XAS measurements at the Eu L_{III} edge. The measurements with varying B content allowed the assignment of the kink to a transition into a mixed valent Eu state. An evaluation of the critical B content resulted in $x_c^{XAS}=0.22\pm0.03$ which is in excellent agreement with the results from XRD and band-structure theory. Furthermore, the temperature independence of the XAS data for a fixed B content above the transition classifies the Eu compounds as heterogeneous mixed valence systems. A heterogeneous mixed valent state is supported by magnetic susceptibility and specific-heat measurements also for higher B concentrations.

To summarize, we could observe a heterogeneous mixed valent state for the compound series $EuPd_3B_x$ for a B content $x_c\gtrsim0.2$ by DFT band-structure calculations, XRD and XAS measurements. Although the calculations do not properly describe the mixed valent scenario, we find remarkably good agreement for the critical B content x_c obtained by the independent methods. In particular, our work demonstrates that the combination of band-structure calculations, modern characterization methods, spectroscopy, and thermodynamical measurements is an ideal tool to gain consistent microscopic insight into the intriguing interplay of crystal chemistry with the electronic and physical properties in intermetallic rare-earth transition metal compounds.

ACKNOWLEDGMENTS

We are indebted to Yu. Grin for valuable discussions, H. Borrmann, Yu. Prots, and S. Hückmann for performing the powder XRD measurements, M. Eckert for WDXS analyses, and P. Simon for advise concerning electron diffraction in the initial phase of this work.

*rosner@cpfs.mpg.de

[1] K. A. Gschneidner Jr., J. Less-Common Met. **17**, 13 (1969).
[2] K. H. J. Buschow, Rep. Prog. Phys. **42**, 1373 (1979).
[3] A. R. Miedema, J. Less-Common Met. **46**, 167 (1976).
[4] F. R. de Boer, W. H. Dijkman, W. C. M. Mattens, and A. R. Miedema, J. Less-Common Met. **64**, 241 (1979).
[5] W. C. M. Mattens, F. R. de Boer, A. K. Nissen, and A. R. Miedema, J. Magn. Magn. Mater. **31-34**, 451 (1983).
[6] J. M. Lawrence, P. S. Riseborough, and R. D. Parks, Rep. Prog. Phys. **44**, 1 (1981).
[7] E. Holland-Moritz, M. Loewenhaupt, W. Schmatz, and D. K. Wohlleben, Phys. Rev. Lett. **38**, 983 (1977).
[8] J. Lawrence, Mod. Phys. Lett. B **22**, 1273 (2008).
[9] R. J. Gambino, W. D. Grobman, and A. M. Toxen, Appl. Phys. Lett. **22**, 506 (1973).
[10] D. Kaczorowski and K. Gofryk, Solid State Commun. **138**, 337 (2006).
[11] A. Pandey, C. Mazumdar, and R. Ranganathan, J. Alloys Compd. **476**, 14 (2009).
[12] A. Pandey, C. Mazumdar, R. Ranganathan, M. De Raychaudhury, T. Saha-Dasgupta, S. Tripathi, D. Pandey, and S. Dattagupta, EPL **84**, 47007 (2008).
[13] D. Music and J. M. Schneider, Appl. Phys. Lett. **89**, 121914 (2006).
[14] A. Pandey, C. Mazumdar, R. Ranganathan, S. Tripathi, D. Pandey, and S. Dattagupta, Appl. Phys. Lett. **92**, 261913 (2008).
[15] J. R. Thompson, S. T. Sekula, C. K. Loong, and C. Stassis, J. Appl. Phys. **53**, 7893 (1982).
[16] A. Pandey, C. Mazumdar, and R. Ranganathan, J. Phys.: Condens. Matter **21**, 216002 (2009).
[17] A. Pandey, C. Mazumdar, R. Ranganathan, V. R. Reddy, and A. Gupta, Appl. Phys. Lett. **94**, 182503 (2009).
[18] S. K. Dhar, S. K. Malik, and R. Vijayaghavan, Mater. Res. Bull. **16**, 1557 (1981).
[19] S. K. Dhar, S. K. Malik, D. Rambabu, and R. Vijayaghavan, J. Appl. Phys. **53**, 8077 (1982).
[20] S. K. Dhar, S. K. Malik, and R. Vijayaraghavan, Phys. Rev. B **24**, 6182 (1981).
[21] S. K. Dhar, R. Nagarajan, S. K. Malik, R. Vijayaraghavan, M. M. Abd-Elmeguid, and H. Micklitz, Phys. Rev. B **29**, 5953

(1984).
[22] S. K. Malik, S. K. Dhar, and R. Vijayaghavan, Bull. Mater. Sci. **6**, 263 (1984).
[23] S. K. Malik, S. K. Dhar, and R. Vijayaghavan, Pramana **22**, 329 (1984).
[24] C. Loison, A. Leithe-Jasper, and H. Rosner, Phys. Rev. B **75**, 205135 (2007).
[25] K. Koepernik and H. Eschrig, Phys. Rev. B **59**, 1743 (1999).
[26] J. P. Perdew and Y. Wang, Phys. Rev. B **45**, 13244 (1992).
[27] H. Eschrig, K. Koepernik, and I. Chaplygin, J. Solid State Chem. **176**, 482 (2003).
[28] A. B. Shick, W. E. Pickett, and A. I. Liechtenstein, J. Electron Spectrosc. Relat. Phenom. **114-116**, 753 (2000).
[29] K. Koepernik, B. Velicky, R. Hayn, and H. Eschrig, Phys. Rev. B **55**, 5717 (1997).
[30] J. A. Blackman, D. M. Esterling, and N. F. Berk, Phys. Rev. B **4**, 2412 (1971).
[31] STOE powder software, WINXPOW, Version 2.08, STOE and Cie GmbH, Darmstadt, Germany, 2003.
[32] L. G. Akselrud, P. Y. Zavalii, Y. N. Grin, V. K. Pecharsky, B. Baumgartner, and E. Wölfel, Mater. Sci. Forum **133-136**, 335 (1993).
[33] J. L. Pouchou and F. Pichoir, in *Electron Probe Quantitations*, edited by K. F. J. Heinrich and D. E. Newbury (Plenum Press, New York, 1991), Vol. 31.
[34] J. Röhler, J. Magn. Magn. Mater. **47-48**, 175 (1985).
[35] Z. Hu, G. Kaindl, and B. G. Muller, J. Alloys Compd. **246**, 186 (1997).
[36] F. Lissner, K. Kramer, T. Schleid, G. Meyer, Z. Hu, and G. Kaindl, Z. Anorg. Allg. Chem. **620**, 444 (1994).
[37] See supplementary material at http://link.aps.org/supplemental/10.1103/PhysRevB.82.235113 for a detailed table including chemical composition from chemical analysis together with the lattice parameters for the synthesized samples.
[38] B. Darshan, B. D. Padalia, R. Nagarajan, S. K. Dhar, S. K. Malik, and R. Vijayaraghavan, Phys. Rev. B **30**, 4031 (1984).
[39] A. Pandey, C. Mazumdar, and R. Ranganathan, J. Magn. Magn. Mater. **322**, 3765 (2010).
[40] P. R. O. Sologub, Intermetallics **18**, 1642 (2010).
[41] J. Roy, J. Am. Ceram. Soc. **37**, 581 (1954).
[42] M. T. Anderson, K. G. Greenwood, G. A. Taylor, and K. R. Poeppelmeier, Prog. Solid State Chem. **22**, 197 (1993).
[43] C. J. Howard, B. J. Kennedy, and P. M. Woodward, Acta Crystallogr., Sect. B: Struct. Sci. **59**, 463 (2003).
[44] T. G. Berger, A. Leineweber, E. J. Mittemeijer, and P. Fischer, Phys. Status Solidi A **201**, 1484 (2004).
[45] B. P. T. Fokwa, Eur. J. Inorg. Chem. **2010**, 3075 (2010).
[46] R. Gumeniuk, M. Schmitt, W. Schnelle, U. Burkhardt, H. Rosner, and A. Leithe-Jasper, Z. Anorg. Allg. Chem. **636**, 954 (2010).
[47] E. R. Bauminger, D. Froindlich, I. Nowik, S. Ofer, I. Felner, and I. Mayer, Phys. Rev. Lett. **30**, 1053 (1973).
[48] E. Sampathkumaran, L. Gupta, R. Vijayaraghavan, K. Gopalakrishnan, R. Pillay, and H. Devare, J. Phys. C **14**, L237 (1981).
[49] I. R. Harris and G. Longeworth, J. Less-Common Met. **23**, 281 (1971).
[50] W. E. Gardner, J. Penfold, T. F. Smith, and I. R. Harris, J. Phys. F: Met. Phys. **2**, 133 (1972).